Journal of Electroanalytical Chemistry xxx (2020) xxx

Contents lists available at ScienceDirect

Journal of Electroanalytical Chemistry

journal homepage: www.elsevier.com/locate/jelechem

Effect of Cu(BDC-NH_2) MOF deposited on Cu/Cu_2O electrode and its better performance in photoelectrocatalytic reduction of CO_2

Beatriz Costa e Silva [a,b,*], Kallyni Irikura [a,b], Regina Célia Galvão Frem [a], Maria Valnice Boldrin Zanoni [a,b]

[a] São Paulo State University (UNESP), Institute of Chemistry, Araraquara. 55 Prof. Francisco Degni St, Araraquara, SP 14800-060, Brazil
[b] National Institute for Alternative Technologies of Detection, Toxicological Evaluation and Removal of Micropollutants and Radioactivies (INCT-DATREM), São Paulo State University (UNESP), Institute of Chemistry, Araraquara, SP 14800-060, Brazil

ARTICLE INFO

Article history:
Received 27 August 2020
Received in revised form 8 November 2020
Accepted 10 November 2020
Available online xxxx

Keywords:
MOF-based electrodes
Cu(BDC-NH_2) prepared by anodic deposition
CO_2 reduction
Photoelectrocatalysis

ABSTRACT

The present work reports the development of Cu/Cu_2O-**Cu(BDC-NH_2)** electrode, prepared by electrochemical deposition using the ligand 2-amino-1,4-benzenedicarboxylic acid and copper ion (II) produced in situ, and its application in CO_2 reduction in aqueous medium. The **Cu(BDC-NH_2)** MOF deposited on Cu/Cu_2O electrode act as efficient catalyst for the photoelectrocatalytic reduction of CO_2 due to its high surface area and high capacity of trapping CO_2. Under optimized conditions and based on the application of the proposed electrode, the photoelectrocatalytic reduction of 0.1 mol L^{-1} sodium sulfate saturated with CO_2 under UV–Vis irradiation and applied potential of +0.1 V can generate an amount of approximately 674 μmol L^{-1} of methanol in 3 h of treatment. The amine substituent in **Cu(BDC-NH_2)** MOF plays an important role in the capturing of CO_2, and this contributes toward obtaining better photoelectrocatalytic efficiency of the CO_2/methanol conversion compared to the use of the Cu/Cu_2O and the non-functionalized Cu/Cu_2O-**Cu(BDC)** MOF electrode.

1. Introduction

Over the past few decades, there have been dramatic advancements in the application of the photoelectrocatalytic technique for CO_2 reduction; this has led several researchers to explore the technique with the aim of finding new alternatives for the conversion of CO_2 into higher value-added products, thus contributing to the reuse of CO_2 emitted into the atmosphere which poses health risks to humans and other living organisms and has been responsible for serious damages to the planet [1–4]. The photoelectrocatalytic technique involves the use of a photocatalyst immobilized on a metallic surface; the outstanding merit of the technique lies in the possibility of using external bias potential to promote better separation of charges (e^-/h^+) photogenerated by irradiation, which improves the efficiency of the process. In spite of its relative success, the potential of the photoelectrocatalytic technique to improve CO_2 reduction depends on the properties of the semiconductor material which has to promote high adsorption of CO_2 on its surface and improve the dissolution of the CO_2 in aqueous medium. Other factors that influence the efficiency of the technique include the applied potential on the semiconductor and the type of photoanode employed (p-type photoanodes are much more preferred because of the greater availability of electrons on the surface). In view of the scarcity of semiconductors with all these properties, many researchers in the field have investigated the use of modifiers immobilized on the surface of semiconductors in order to equip them with the desirable electrochemical properties [5–7]. Among the modifiers that deserve being mentioned include those that increase CO_2 adsorption on semiconductor surfaces, increase the effectiveness of light collection, amplify the use of light spectrum and solar radiation, in addition to increasing the limited solubility of CO_2 in aqueous solution. Essentially, these modifiers have been employed aiming at reducing the set-up and operational costs of the photoelectrocatalytic reactor, while increasing the selectivity and efficiency of the method.

The use of metal-organic frameworks (MOFs) as catalysts for CO_2 reduction has gained considerable traction in the last few years [8,9]. MOFs are a new class of nanopore crystalline hybrid materials formed by the coordination of compounds in three-dimensional structure combining organic binders with metallic ions. These frameworks have gained remarkable popularity as an ideal platform for CO_2 capture due to their large surface area, in addition to possessing structures with pore sizes and CO_2-adjustable functionality [10]. The electrochemical deposition of thin MOF films on metallic electrodes has been increasingly studied in the field and a number of studies published in the literature have demonstrated a wide range of advantages related to the application of this mechanism. Among the outstanding advantages of MOF-based electrodes are as follows: (i) they are easy to obtain [11,12]; (ii) they do not need substrate pretreatment, which reduces deposition time and simplifies the procedure [13]; (iii) they are

* Corresponding authors at: São Paulo State University (UNESP), Institute of Chemistry, Araraquara. 55 Prof. Francisco Degni St, Araraquara, SP 14800-060, Brazil.
E-mail addresses: beatriz.cs@gmail.com, (B.C. Silva), boldrinv@iq.unesp.br. (M.V.B. Zanoni).

http://dx.doi.org/10.1016/j.jelechem.2020.114856

characterized by rapid formation [10,14]; (iv) they involve mild reaction conditions [15]; (v) they help monitor the deposition process, which allows greater control of film thickness [16]; and (vi) MOF-based methodologies are an environmentally friendly processes, once the use of large quantities of metals and disposal of metal salts are eliminated in the case of anodic deposition. Despite their suitable properties, there have been scarce reports in the literature regarding the use of these MOFs as co-catalysts deposited on semiconductors with a view to improving the photoelectrocatalytic process. As pointed out in the literature, some of these MOF materials are capable of photoeletrocatalytically producing hydrogen and/or oxygen by water splitting [17–22], apart from promoting CO_2 reduction [5,23–25] and organic compounds degradation [26]. The main drawback of MOF-based electrodes is that the application of these electrodes has often resulted in low overall energy conversion efficiency and most of the MOF-based methodologies proposed in the literature are seen to be far from practical application.

Thus, the present work investigates the construction of **Cu(BDC-NH$_2$)** MOF (Fig. 1) on Cu/Cu_2O electrode via electrochemical deposition of the ligand 2-amine-1,4-benzenedicarboxylic acid (1,4-BDC-NH_2). The addition of amine substituent in a three-dimensional structure can give rise to new binding sites and help improve the capture of CO_2 through its absorption by the amine group that is a weak basic site. The capture of carbon dioxide occurs through specific interaction and improve the pre-concentration of CO_2 on the p-type semiconductor, such as Cu_2O. The applied potential is optimized aiming at improving the conversion and recycling of CO_2 into products of higher added value via photoelectrocatalytic reduction.

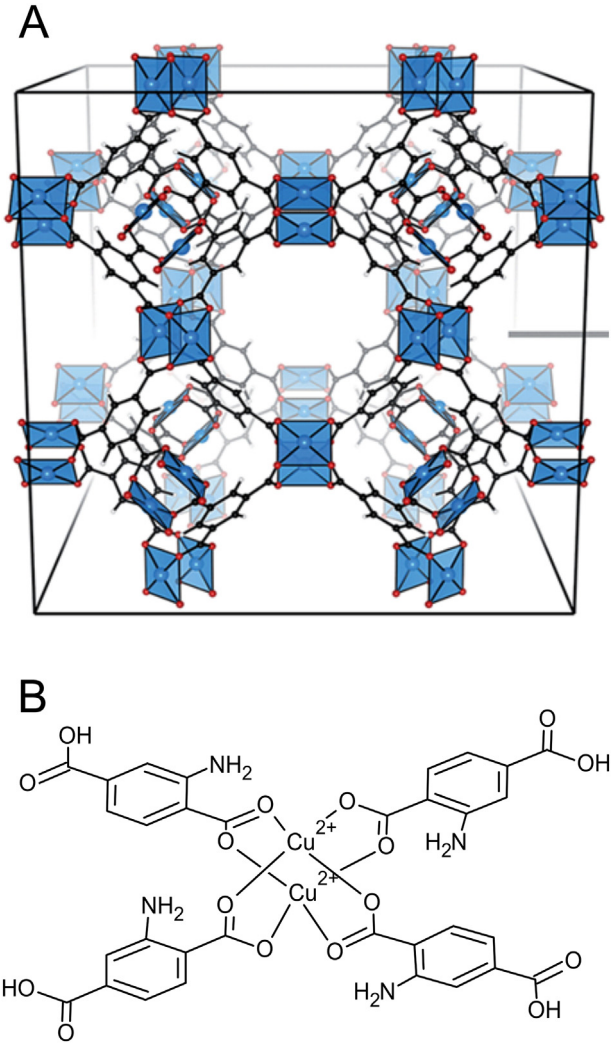

Fig. 1. Cu(BDC-NH$_2$) MOF cubic structure (A), Cu_2L_4 paddle-wheel secondary building unit (B).

2. Experimental

2.1. Chemicals

N,*N*-dimethylformamide (J. T. Baker, 99,9%), 2-amine-1,4-benzenedicarboxylic acid (acquired from Sigma Aldrich, 98%), glacial acetic acid (acquired from Quemis, 99,7%), nitric acid (obtained from J. T. Baker, 65,7%) and ultra-pure water (Milli-Q) were used for conducting the synthesis. Copper foil (0.10 mm thick, 99.5%) was cleaved (3.0 × 3.0 cm^2) and rinsed with acetone, isopropyl alcohol and water prior to use.

2.2. Synthesis of Cu/Cu_2O-**Cu(BDC-NH$_2$)** electrodes

The synthesis of Cu/Cu_2O-**Cu(BDC-NH$_2$)** MOF (Fig. 2) was performed by immersing two copper foils previously immersed in a 905 mg 2-amine-1,4-benzenedicarboxylic acid (1,4-H_2BDC-NH_2) solution dissolved in a solution containing 50 mL dimethylformamide (DMF), 2.860 mL of glacial acetic acid, 600 μL of nitric acid, and 180 μL of water; this synthesis method employed here was based on the method described in the literature [27]. The synthesis was conducted under controlled current of 2.5 mA cm^{-2} with variation of the anodization time from 4.0 to 45 min at 110 °C under stirring (Table 1). Afterwards, the electrode was washed with water and dried at 100 °C for 24 h after anodization.

2.3. Characterization of Cu/Cu_2O-**Cu(BDC-NH$_2$)** electrodes

The crystallinity of the **Cu(BDC-NH$_2$)** powder was evaluated by X-Ray diffraction (XRD), using Siemens D5000 diffractometer (Siemens, Munich, Germany) with Cu-Kα radiation, controlled by DIFFRAC and XRD Commander software.

Optical properties of Cu/Cu_2O-**Cu(BDC)** electrodes and **Cu(BDC-NH$_2$)** powder were evaluated by absorbance of the material in the range of 200 to 800 nm using a Cary 60 UV–Vis spectrometer (Agilent Technologies, Santa Clara, CA, USA) equipped with an external probe accessory (acquired from Barrelino, Harrick Scientific, Pleasantville, NY, USA). The product was calibrated with standard Spectralon (Labsphere USRS-99-020, 99% reflectance).

The morphological characterization of Cu/Cu_2O-**Cu(BDC-NH$_2$)** electrodes was performed using a field scanning electron microscope (FEG-SEM), Mark JEOL, model JSM-7500F (JEOL, Tokyo, Japan), with the aid

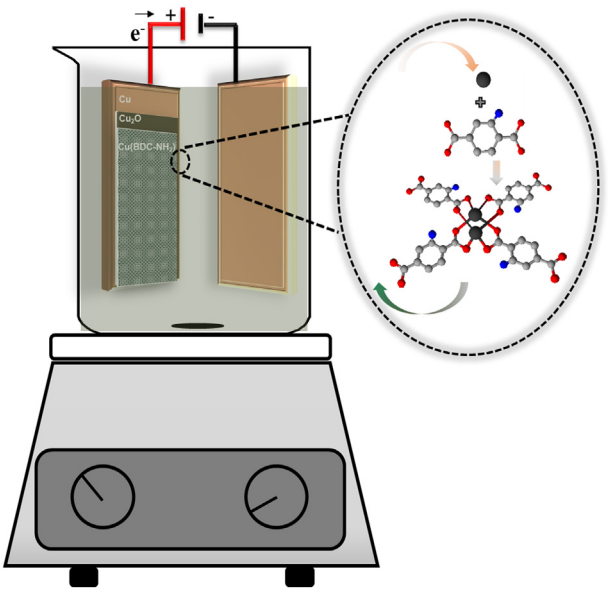

Fig. 2. Illustration of the synthesis of Cu/Cu_2O-**Cu(BDC-NH$_2$)** electrodes by anodic electrochemical deposition.

Table 1
Cu/Cu_2O-**Cu(BDC-NH_2)** electrodes synthesized in different conditions.

Electrodes	Current density (mA cm^{-2})	Anodization time (min)	Temperature (°C)
1	2.5	45	110
2	2.5	30	110
3	2.5	6.5	110
4	2.5	4.0	110

of PC-SEM version 2.1.0.3 operating software, with side-circuit detectors, backscatter, and gold spectrometer (EDS) - Thermo Scientific Ultra Dry model with NSS 2.3 operating software.

Fourier transform infrared (FTIR) vibrational spectra were obtained from Bruker Vertex 70 spectrophotometer (Bruker, Ettlingen, Germany) equipped with a LADTGS detector, in the range of 4000 to 400 cm^{-1}. The ATR measurements were performed using the attenuated total reflection medium (diamond crystal) and the infrared reflection spectroscopy (DRIFTS) analysis was conducted in the absence and presence of CO_2 under 5 atm pressure for 24 h.

Photocurrent vs potential curves in the dark, under UV–Vis, and by only visible irradiation were recorded through the application of linear scan voltammetry at scan rate of 100 mV s^{-1} using an Autolab PGSTAT 128 N potentiostat/galvanostat (Metrohm, Herisau, Switzerland).

2.4. Reactor

The analysis of photocatalysis (PC), electrocatalysis (EC) and photoelectrocatalysis (PEC) were carried out in stainless-steel reactor with a total volume of 150 mL where the source of illumination helped ensure the reproducibility of the measurements (Fig. 3). There was a 1.0 cm distance between the electrodes and a 5 cm diameter quartz side window at a distance of 1.0 cm from the working electrode. The pressure of the system was controlled with manometer and kept constant at 1 atm. The solution was stirred using a magnetic bar at the base of the reactor.

2.5. CO_2 reduction experiments

The following techniques were applied for the CO_2 reduction experiments: photoelectrocatalysis (PEC), photocatalysis (PC), and electrocatalysis (EC). The PEC and EC experiments were conducted under a controlled potential using Cu-MOF as the working electrode (3.0 × 3.0 cm^2). DSA® plate was employed as counter electrode while 4.0 mol L^{-1} KCl containing Ag/AgCl was used as reference electrode. The working electrode was illuminated by UV–Vis and visible light (with the inclusion of a lens to filter the UV) using xenon arc lamp (ORIEL, 300 W). The same reactor was employed for performing the PC experiments using UV–Vis and visible light irradiation as catalyst but without the application of potential. The 0.1 mol L^{-1} Na_2SO_4 supporting electrolyte was CO_2-saturated (Oxi-Ara, São Paulo, Brazil) prior to each experiment; this was done by bubbling CO_2 in the solution for 20 min with a diffuser gas system to improve mass transfer of the gas and reduce the bubble size. After this procedure, the reactor was sealed and the pressure was kept at 1 atm.

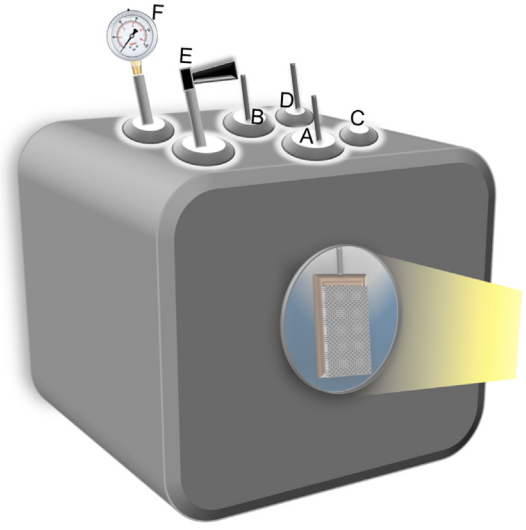

Fig. 3. Photoreactor used in all the experiments. (A) Working electrode, (B) counter electrode, (C) septum, (D) reference electrode, (E) CO_2 inlet and outlet, and (F) manometer.

2.6. Identification and quantification of the products generated during CO_2 reduction

The products formed through CO_2 reduction was identified and quantified by gas chromatography with flame ionization detection (GC-FID) using Shimadzu 2010 model equipment. For the analysis of the samples, extraction of the products was performed by transferring a 0.5 mL aliquot solution to a sealed 1.5 mL vial and heating the solution in a bath for 7 min at 65 °C. Subsequently, a 75 μm Carboxen / PDMS fiber (Supelco) was exposed to the vapor in the vessel for 5 min; the fiber was then injected in the gas chromatograph. A Restec Stabilwax chromatographic column (30 m × 0.25 mm id; 25 μm thickness) was used in this analysis. Nitrogen at a flow rate of 1.0 mL min^{-1} was employed as carrier gas. The injector was operated at 250 °C without input and the detector temperature applied was 260 °C. The heating program of the column furnace was subjected to an initial temperature of 40 °C, followed by heating at 2 °C min^{-1} at 46 °C and then at 45 °C min^{-1} at 170 °C, maintaining the final temperature for 3 min. The quantification of the compounds was conducted using analytical curves constructed previously for each compound: acetone (time (t) = 3.2 min; regression equation (y) = 3105.01x + 20,103; and determination coefficient (r^2) = 0.997), methanol (t = 3.7 min; y = 6.0451x + 328.97, r^2 = 0.983) and ethanol (t = 4.0 min; y = 125.06x + 852.17, r^2 = 0.993). All measurements were performed in triplicate in 0.1 mol L^{-1} sodium sulfate solution at concentrations ranging from 1 to 100 (acetone); 10 to 1000 (methanol); and 10 to 1000 μmol L^{-1} (ethanol).

3. Results and discussion

3.1. Synthesis and characterization of **Cu(BDC-NH_2)** powder and Cu/Cu_2O-**Cu(BDC-NH_2)** electrodes

The surface morphology of the Cu/Cu_2O-**Cu(BDC-NH_2)** electrodes can be observed through the FEG-SEM images presented in Fig. 4. One can visualize the surface covered by the cubic planar nanocrystal and/or microcrystal particles, with sizes ranging from 1.47, 1.21, 1.00 to 0.79 μm for electrodes 1 (A), 2 (B), 3 (C), and 4 (D), respectively. For a comparison of the morphology of the thin films, Fig. 5 (Curves E and F) presents the FEG-SEM images of Cu/Cu_2O electrode formed as a model electrode in the absence of BDC-NH_2 ligand. The crystals grown in the presence of the ligand exhibited different geometries and morphologies associated with the film formed on the Cu substrate; this confirms the formation of different coatings on the electrode. The dimensions of **Cu(BDC-NH_2)** changed from 0.87 and 0.19 to 1.67 and 0.87 μm for electrodes 2 (30 min) and 3 (6.5 min), respectively.

The MOF film formed on the electrode in 45 min of electrolysis was found to be very thick and slightly adherent; also, the film formed in 4 min of the process did not cover the whole surface of the electrode; as such, both films were discarded. The film formed in 30 min of electrolysis covered the surface of the copper electrode and the film formed in 6.5 min of electrolysis was found to be very fine; as a result, both films were chosen for the conduct of CO_2 reduction by photocatalysis and photoelectrocatalysis.

The Cu/Cu_2O-**Cu(BDC-NH_2)** electrodes were subjected to energy dispersive X-ray spectroscopy (EDS) analysis (Fig. 5). The spectral analysis indicated the presence of peaks attributed to copper, oxygen, nitrogen and

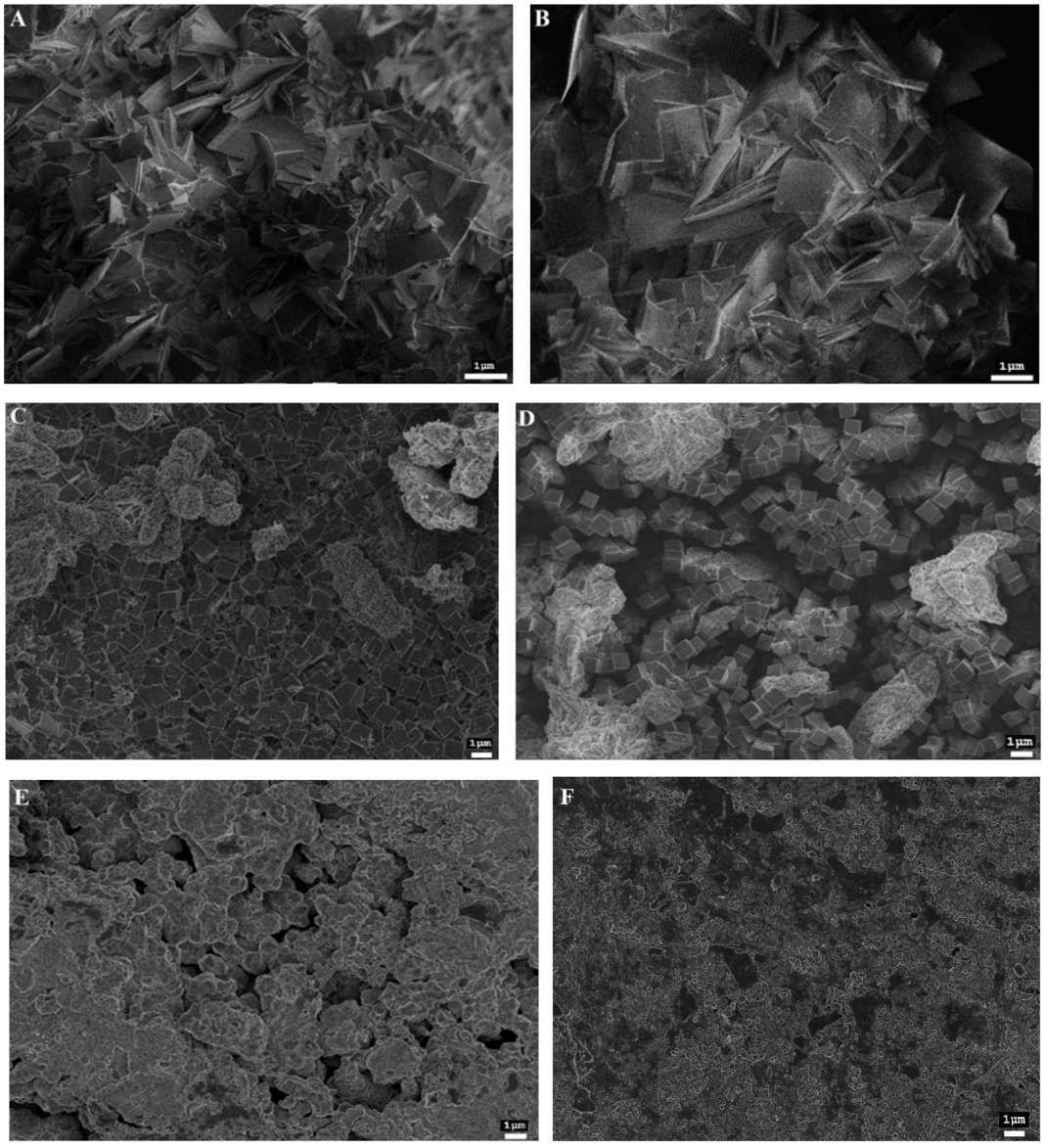

Fig. 4. FEG-SEM images of Cu/Cu_2O-**Cu(BDC-NH_2)** electrodes formed, after 45 (A), 30 (B), 6.5 (C) and 4 min (D) of anodization at controlled current density of 2.5 mA cm^{-2}, under controlled temperature of 110 °C, in the presence of 905 mg of ligand; and (E) images of Cu/Cu_2O electrode after 30 and (F) 6.5 min of anodization under the same conditions but in the absence of the ligand.

carbon; this pointed to the presence of the ligand (H_2BDC-NH_2) in the MOF on the copper oxide grown on the surface of the metallic copper.

The X-ray diffraction (XRPD) analysis enables one to determine the amorphous or crystalline nature of the substances and to verify the success

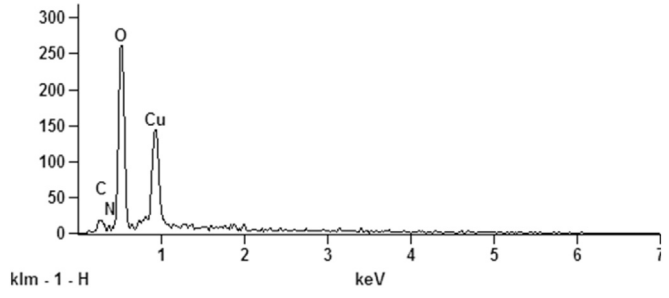

Fig. 5. EDS of Cu/Cu_2O-**Cu(BDC-NH_2)** electrode prepared under current density of 2.5 mA cm^{-2}, anodization time of 30 min, and temperature of 110 °C.

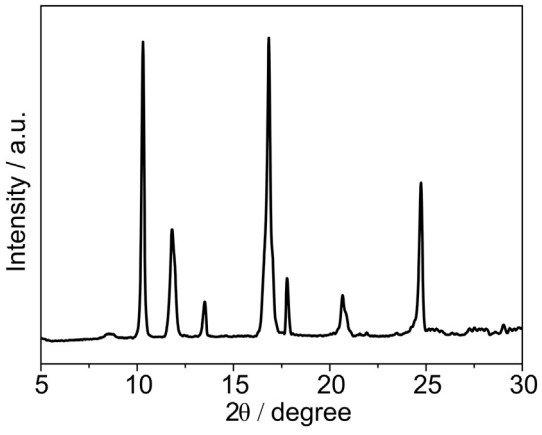

Fig. 6. XRPD patterns of **Cu(BDC-NH_2)** powder.

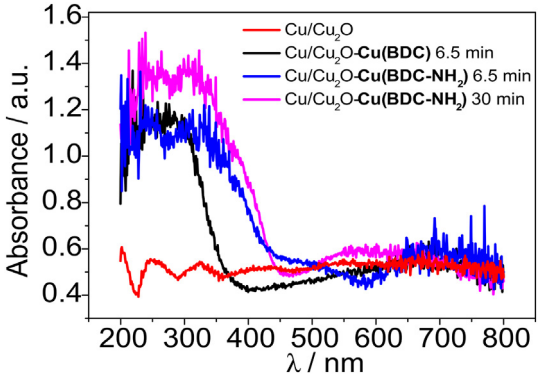

Fig. 7. UV–Vis reflectance spectra of Cu/Cu_2O-**Cu(BDC-NH_2)** electrodes prepared in 6.5 (blue) and 30 min (pink) of anodization; Cu/Cu_2O-**Cu(BDC)** electrode prepared in 6.5 min (black) of anodization; and Cu/Cu_2O prepared in 30 min of anodization in the absence of the ligand.

or failure to obtain the desired phase. The characteristic peaks observed at 2θ = 10.30°, 11.84°, 16.82°, 20.67° and 24.73° pointed to the crystalline nature of the microcrystalline **Cu(BDC-NH_2)** (Fig. 6). The observed XRPD spectra are in good agreement with the reports in the literature [9].

3.2. Optical properties of Cu/Cu_2O-*Cu(BDC-NH_2)* electrodes

The optical properties of Cu/Cu_2O-**Cu(BDC-NH_2)** electrodes were investigated by reflectance spectra analysis; the data are shown in Fig. 7. The spectra of Cu/Cu_2O-**Cu(BDC-NH_2)** systems (electrodes 2 and 3) presented well defined absorption bands in the UV–Vis and visible regions, with high absorptions at ~250 and 330 nm (see below), attributed to ligand-centered transitions, and $d_{x2-u2} \rightarrow$-*dxz,yz* copper(II) transitions corresponding to the broad and distorted bands in the 560 and 800 nm spectral range [28]. For the electrode prepared under the same experimental conditions as electrode 3 but using MOF with non-functionalized BDC ligand (see black line in Fig. 7), the spectrum exhibited no significant change in terms of absorption behavior [29]. An assessment of the Cu/Cu_2O-**Cu(BDC)** electrode prepared in anodization time of 6.5 min was found to essential because this electrode presented the best conversion of CO_2/methanol; hence, a study of the electrode will enable one to better understand the effect of functionalization by the presence of the amine ligand. The presence of a second intra-ligand band (~ 330 nm) in the spectra of the electrodes constructed with functionalized MOFs (lines blue and pink of Fig. 7) is attributed to the fact that the nitrogen lone pair of the NH_2 group in the organic ligand introduces a new electronic transition populating the π* orbitals of the benzene ring, thus donating electron density to the anti-bonding orbitals [30].

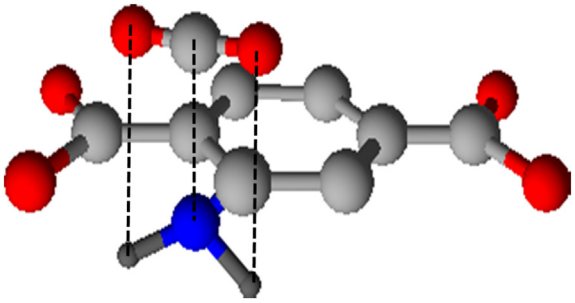

Fig. 9. Interactions of CO_2 with the amine group of **Cu(BDC-NH_2) MOF.** Red: H, grey: C and blue: N.

3.3. Cu/Cu_2O-*Cu(BDC-NH_2)* electrode performance in the presence of CO_2

The ATR infrared analysis was carried out in order to confirm the formation of **Cu(BDC-NH_2)** MOF [9] on the surface of the electrode through the evaluation of vibrational transitions in the spectral range of 4000 to 400 cm^{-1}. As can be seen in Fig. 8A, two bands are observed at the beginning of the spectrum at 3227 and 3144 cm^{-1}, corresponding to the -NH_2 stretching vibrations. As expected, the main infrared bands of the organic ligand are observed in the spectra, with the remarkable presence of the bands corresponding to the vibrational modes $\upsilon_{as}COO^-$ (1593 cm^{-1}), υ_sCOO^- (1373 cm^{-1}), νC-O-Cu (1124 cm^{-1}) and the CuO stretching vibration at 514 cm^{-1}, in addition to the bands observed in the range of 2969–2822 cm^{-1} attributed to CH stretching vibrations. When the **Cu(BDC-NH_2)** MOF is exposed to CO_2, one notices the presence of infrared MOF bands and the typical bands related to carbon dioxide molecule, such as the combinational bands ν3 + ν1 and ν3 + 2ν2 (3732 and 3623 cm^{-1}, respectively) and the asymmetric υ3 CO_2 stretching bands at 2361 and 2341 cm^{-1}; this implies that the MOF-based electrode presented efficient gas adsorption.

The results of a comparative FTIR-ATR study regarding the behavior of the electrodes in the presence of CO_2 are shown in Fig. 8B. In addition to the absorption bands related to the vibrational modes of the organic ligands (see discussion above), in the presence of CO_2, one notices the presence of typical bands of carbon dioxide molecules such as the combination bands (3705 and 3697 cm^{-1}) and the bands associated with the asymmetric υ3 stretching mode at 2341 and 2360 cm^{-1} for all the MOF-based electrodes. Once again, looking at Fig. 8B, one can clearly observe the presence of CO_2 ν_{as} bands in the spectra of the Cu/Cu_2O-**Cu(BDC-NH_2)** electrodes with a

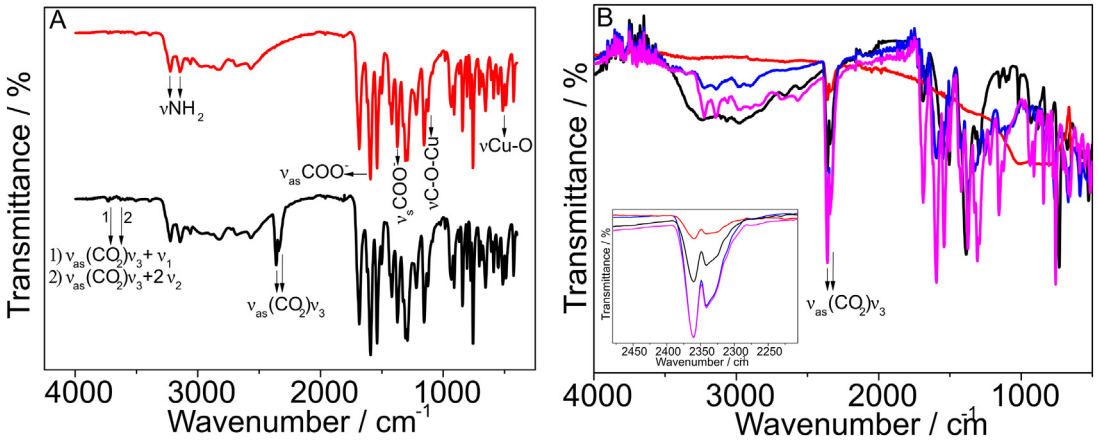

Fig. 8. (A) FTIR-ATR spectra of **Cu(BDC-NH_2)** in the absence (red) and presence (black) of CO_2 and (B) Cu/Cu_2O-**Cu(BDC-NH_2)** electrodes 2 (pink) and 3 (blue), Cu/Cu_2O-**Cu(BDC)** (black) and Cu/Cu_2O (red) electrodes after 24 h of exposure to CO_2. *Inset*: amplified region of CO_2 asymmetric (υ3) stretching bands.

relatively higher intensity; this points to a better gas adsorption capacity for the amine-functionalized materials in relation to the electrode Cu/Cu_2O-**Cu(BDC)** [29].

The interaction of CO_2 with terephthalic acid in the MOF cavities occurs preferably in a more stable way on top of the benzene ring (BE = −10.651 KJ mol^{-1}), in addition to the interaction on top of the acid group (BE = −7.470 KJ mol^{-1}). Furthermore, a more stable interaction of CO_2 with aminoterephthalic acid occurs on top of the amine group (BE = −12.728 KJ mol^{-1}) alongside the interaction on top of the benzene ring (BE = −10.191 KJ mol^{-1}) or on top of the acid group (BE = −8.782 KJ mol^{-1}) [31]. Fig. 9 shows the preferential interaction sites of CO_2 with the amine group of the functionalized MOF amine.

The high CO_2 absorption observed for the electrodes constructed with **Cu(BDC-NH_2)** MOF suggests a strong interaction between carbon dioxide molecules and the MOF. According to the literature, the main interaction sites must involve the $C^{\delta+}...N^{\delta-}$ electrostatic bond and NH_2...OCO hydrogen bonding [32,33], which will boost the occurrence of photocatalysis.

3.4. Photoactivity of Cu/Cu_2O-**Cu(BDC-NH_2)** electrodes

Fig. 10 compares the linear scan voltammograms obtained for Cu/Cu_2O-**Cu(BDC-NH_2)** electrode prepared in 30 min of anodization at 2.5 mA cm^{-2} in 0.1 mol L^{-1} Na_2SO_4, in the potential range of 0 to −1.5 V (A and C) and 0 to 1.0 V (B and D), with scan rate of 10 mV s^{-1}, in the dark (curve a), before (curve b) and after saturation with CO_2 (curve c) and subject to UV–Vis (A and B) and visible light irradiation (C and D).

As can be noted in Fig. 10, the reduction of **Cu(BDC-NH_2)** MOF in the dark (curve a) presents a well-defined peaks sets around −0.60 and − 0.75 V attributed to the reduction of Cu(II)/Cu(I) and Cu(I)/Cu (0) in the complex. The evolution curves of hydrogen can be observed in potentials more negative than −1.1 V.

The photocurrent recorded for Cu/Cu_2O-**Cu(BDC-NH_2)** electrode when irradiated by both UV–Vis or visible light (curve b) are smaller and a small peak is observed around −0.5 V and −0.25 V, respectively. According to the literature [34], when a semiconductor is irradiated with light energy greater than that of the band gap, electron–hole pairs are generated on the electrode surface and the photocurrent reflects the charge separation on the electrode interface. Thus, under irradiation the metallic center could be reduced in the MOF preferentially by the photogenerated electrons [2] and the original peaks of the metal is not seen in the voltammogram, since the shape of the photocurrent voltammograms reflects the balance between the recombination of electron–hole pairs and substrate photoreduction (water in this case).

But, for Cu/Cu_2O-**Cu(BDC-NH_2)** electrode when irradiated by both UV–Vis or visible light with CO_2-saturated electrolyte is observed a higher photocurrents and marked peaks around −0.35 V and −0.80 V (curve c). Taking into account that the pH is slightly changed from pH 6.8 to pH 4.5 and CO_2 could be adsorbed on MOF cavities as diagnosed previously many photoelectrocatalytic reactions could takes places like Cu(II) reduction, ligand reduction, hydrogen synthesis and also CO_2 reduction. But, this behavior shows that e^-/h^+ pairs are been generated under both visible and UV irradiation and the application of a potential increases the efficiency of these charge separation. For this, further photoelectrolysis were carried out and hydrogen evolution and methanol, ethanol and other sub-products were analyzed.

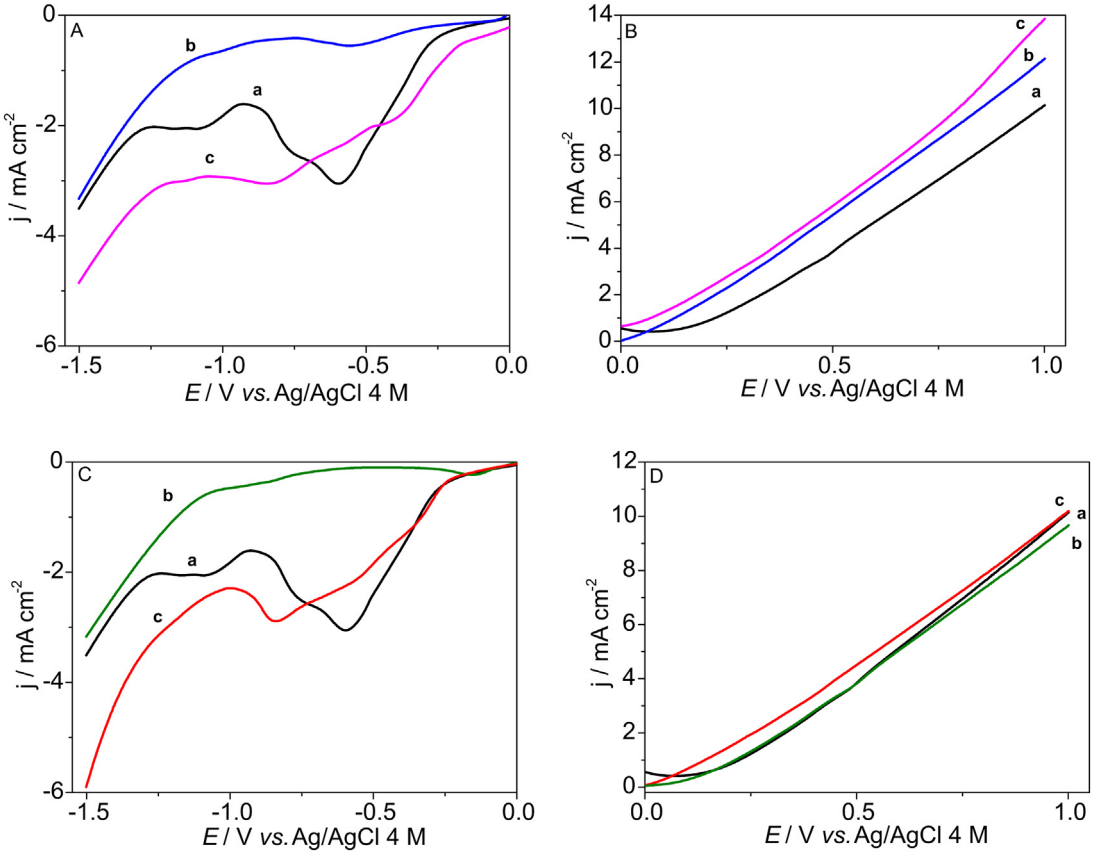

Fig. 10. Linear scan voltammograms at Cu/Cu_2O-**Cu(BDC-NH_2)** prepared during 30 min (electrode 2) in 0.1 mol L^{-1} Na_2SO_4 in the dark (a), irradiated by UV–Vis (A and B) and visible light (C and D) without CO_2 (b) and saturated with CO_2 (c). Scan rate = 10 mV s^{-1}.

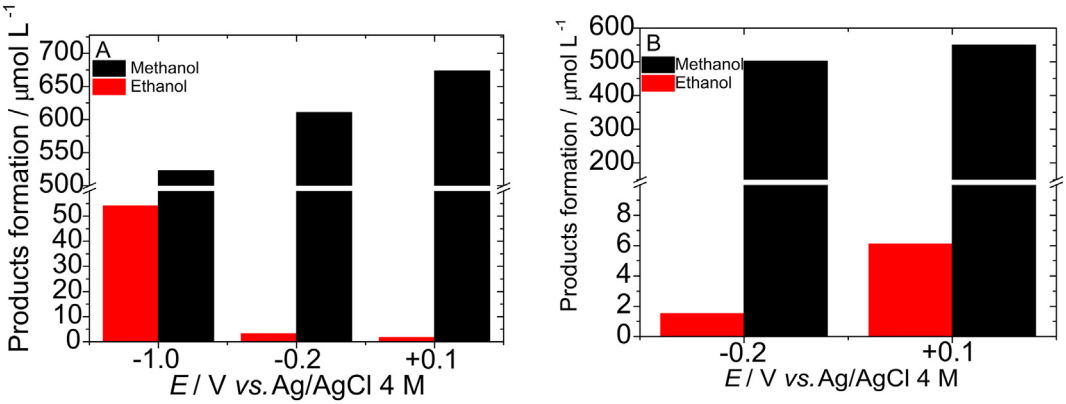

Fig. 11. Evaluation of the potential relative to the concentration of methanol and ethanol formed during the photoelectrocatalytic reduction of CO_2 for Cu/Cu_2O-**Cu (BDC-NH_2)** electrodes 2 (A) and 3 (B) applied toward PEC at +0.1 V, under UV–Vis irradiation in 0.1 mol L^{-1} Na_2SO_4.

The voltammetric behavior of the electrodes was investigated under positive potentials ranging from 0 to +1.0 V, in the absence and presence of CO_2, to avoid the reduction of metal ions Cu(II) in the MOF under UV–Vis and visible and dark irradiation (Fig. 10B and D). In the presence of light and CO_2, voltammograms showed an increase in photocurrent (curve c). This behavior shows that e^-/h^+ pairs are generated under UV–Vis irradiation and the application of a potential increases the efficiency of charge separation. The potential of +0.1 V was studied so that there would be no competition with the O_2 shedding reaction which is a competitive with CO_2 reduction.

3.5. Photoelectrocatalytic reduction of CO_2

Fig. 11 shows the concentration of methanol and ethanol formed through photoelectrocatalytic reduction of CO_2 on Cu/Cu_2O-**Cu(BDC-NH_2)** electrodes in saturated solution of 0.1 mol L^{-1} sodium sulfate by photoelectrolysis conducted at controlled applied potentials of −1.0, −0.2 and + 0.1 V under UV–Vis irradiation. CO and CH_4 gases, formiate and acetone were also evaluated, but their occurrence was below to the detection limit of the method in the samples collected. With regard to electrode 2, methanol formation was found to be much lower at negative potential around −1.0 (522.91 µmol L^{-1}), in relation to less negative potential at −0.2 V (610.41 µmol L^{-1}) and positive potential at +0.1 V (673.77 µmol L^{-1}). The results show that CO_2 conversion occurs relatively more efficient under positive potentials; this is because at negative potentials one observes the occurrence of a competition between CO_2 reduction and hydrogen evolution. With regard to electrode 3, compared to the amounts of methanol and ethanol formed under positive potentials (549.70 µmol L^{-1} of methanol and 6.10 µmol L^{-1} of ethanol), relatively lower amounts of methanol (502.23 µmol L^{-1}) and ethanol (1.52 µmol L^{-1}) were formed at the negative potential of −0.2 V. The results show that the reduction of CO_2 /methanol conversion on thinner films is at least 1.2 times lower than when the process involves the use of film formed in 30 min of MOF electrodeposition. The thickness of the MOF film exerted a direct influence over the photoelectrocatalytic conversion of CO_2, which is measured by the amount of methanol and ethanol generated on electrodes 2 and 3. Although electrode 3 exhibited a smaller surface area (Fig. 12B), the coating on the electrode surface was found to be neither homogeneous nor complete, and this undermined the photoelectrocatalytic reduction by MOF. Interestingly, despite possessing a relatively larger surface area, electrode 2 presented greater coating on the electrode surface (Fig. 12A) with the presence of a greater amount of MOF; as such, there was a much greater number of cavities available for CO_2 to be trapped and converted to methanol and ethanol.

An assessment of the results obtained for Cu/Cu_2O and Cu/Cu_2O-**Cu(BDC)** electrodes prepared in 6.5 min of anodization shows that CO_2 reduction generated 234 and 11.36 µmol L^{-1} methanol for the latter and the former [29], respectively; these results are at least 2 and 4 times lower, respectively, when compared with the result

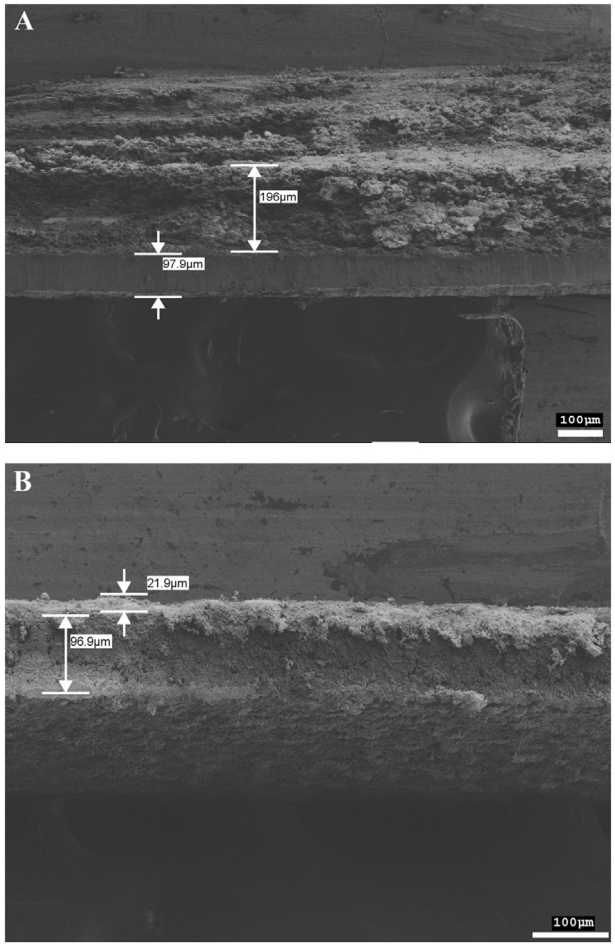

Fig. 12. FEG-SEM cross-section images of Cu/Cu_2O-**Cu(BDC-NH_2)** electrodes 2 and 3 formed in 30 (A) and 6.5 min (B) of anodization time, at controlled current density of 2.5 mA cm^{-2}, and controlled temperature of 110 °C.

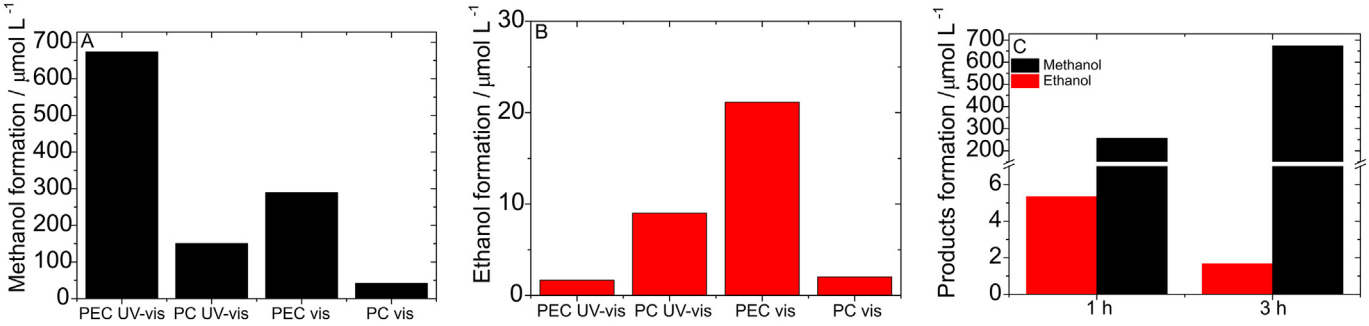

Fig. 13. Concentration of (A) methanol and (B) ethanol formed during the photoelectrocatalytic and photocatalytic reduction of CO_2 on Cu/Cu_2O-**Cu(BDC-NH_2)** electrode 2 in 0.1 mol L^{-1} Na_2SO_4 irradiated with UV–Vis and visible irradiation under applied potential of +0.1 V (PEC) and without potential (PC). (C) Effect of time on methanol and ethanol formation during photoelectrocatalytic reduction of 0.1 mol L^{-1} Na_2SO_4 saturated with CO_2 on Cu/Cu_2O-**Cu(BDC-NH_2)** electrode 2 under applied potential of +0.1 V and UV–Vis irradiation.

obtained for Cu/Cu_2O-**Cu(BDC-NH_2)** electrode formed in solution under the same conditions. With regard to Cu/Cu_2O-**Cu(BDC)** and Cu/Cu_2O electrodes prepared in 30 min of anodization time, the amounts of methanol formed were 50.4 and 16.2 μmol L^{-1}, respectively; these values are at least 13 and 42 times lower, respectively, compared to the value obtained for the Cu/Cu_2O-**Cu(BDC-NH_2)** electrode. The results illustrate the importance of the use of **Cu(BDC-NH_2)** for improving the electrode performance; clearly, amine sites are highly effective for CO_2 adsorption and can act as light-absorption chromophores [35].

3.5.1. Effects of irradiation and photoelectrolysis time on CO_2 reduction

Wavelength spectrum and light intensity are crucial factors when one seeks to obtain an efficient photoelectrocatalysis process. In addition, the irradiation wavelength is another important factor that can affect the efficiency of the process. The use of solar light is found to be challenging in the sense that the widest wavelength region of the spectral distribution of sunlight in air consists of photons with wide wavelengths ranging from ultraviolet (UV) to infrared (IR), but with more light intensity at visible region [36]. Thus, in order to test the versatility of irradiation on Cu/Cu_2O-**Cu(BDC-NH_2)** electrodes, the photoelectrocatalytic reduction of CO_2 was carried out in 0.1 mol L^{-1} Na_2SO_4 saturated with CO_2 during the photoelectrocatalytic and photocatalytic reduction of CO_2 under visible and UV–Vis irradiation. The results obtained after 3 h of treatment are shown in Fig. 13.

An amount of approximately 674 μmol L^{-1} of methanol was formed through the application of PEC under UV–Vis irradiation, while a relatively lower yet significant amount of 289 μmol L^{-1} of methanol was also obtained when visible light was applied. In comparison with the amount of methanol formed, the amount of ethanol formed in the process can be considered negligible. The findings of the present study are essentially remarkable in the sense that they show that the proposed electrode responds favorably when irradiated by UV–Vis light.

The results show that the application of photocatalysis without bias potential leads to up to 77% decline in the electrode performance in terms of methanol generation; this indicates that the simultaneous external potential increases the band bending on the electrode surface, which, consequently, increases the electron transfer efficiency in CO_2 adsorption. The results also show that the sole application of the electrocatalytic process did not result in the formation of any products.

Thus, through the application of the optimized experimental conditions, the formation of methanol and ethanol was evaluated after 1 and 3 h of phooelectrocatalysis using Cu/Cu_2O-**Cu(BDC-NH_2)** electrode in 0.1 mol L^{-1} Na_2SO_4 saturated with CO_2, under UV–Vis irradiation, with applied potential of +0.1 V. The results obtained are shown in Fig. 13C. As can be observed, it is clear that the formation of ethanol decreases after a longer period of treatment. By contrast, the formation of methanol is seen to increase over time, reaching up to 674 μmol L^{-1}; this shows that the process depends on the duration of photoelectrolysis.

Based on these results, one can conclude that the capture of CO_2 by the growth of **Cu(BDC-NH_2)** MOF on the electrode surface and the higher absorption of energy photons by the MOF lead to the enhancement of the trapping of electrons on the Cu/Cu_2O surface under irradiation. The pre-concentration of CO_2 on the electrode surface due to strong interaction with the nitrogenated sites of the –BDC-NH_2 groups makes the conversion of CO_2 into methanol more efficient via photoelectrocatalytic reduction. The process is represented in Scheme 1.

Fig. 14A presents the FEG-SEM images of Cu/Cu_2O-**Cu(BDC-NH_2)** electrode after 3 h of photoelectrocatalysis for CO_2 reduction in the presence of UV–Vis irradiation in 0.1 mol L^{-1} Na_2SO_4. It is possible to observe that the morphological change on the electrode surface after the photoelectrocatalysis was slightly changed. But, the amperometric behavior of the photoelectrode was analyzed before and after 3 h of photoelectrocatalysis and the results shown in Fig. 14B. There is no significant variation in the current density at least during three photoelectrocatalysis, suggesting that the electrode efficiency is good when the electrode is reused.

4. Conclusion

The present study showed that Cu/Cu_2O-**Cu(BDC-NH_2)** electrode prepared by electrochemical deposition acts as a good platform for CO_2 preconcentration via interaction with 2-amine,1,4-benzenedicarboxylic acid. The results show that 30 min of anodization and current density of 2.5 mA cm^{-2} are the best experimental conditions for obtaining a material with excellent photoelectrocatalytic activity. Furthermore, compared to non-functionalized electrodes, in which amine groups are absent, the introduction of amine substituent in the MOF film has been found to boost the adsorption of CO_2. The proposed Cu/Cu_2O-**Cu(BDC-NH_2)** electrode presented higher photoelectrocatalytic reduction of CO_2 in 0.1 mol L^{-1} sodium sulfate applied under UV–Vis radiation with bias potential of +0.1 V; the use of this electrode led to the formation of an amount of 674 μmol L^{-1} of methanol after 3 h of treatment, with high stability and better performance in relation to other electrodes. The results obtained illustrate that the growth of **Cu(BDC-NH_2)** MOF on Cu/Cu_2O electrode led to an increase in the conversion of CO_2 to methanol almost 42 times in relation to Cu/Cu_2O electrode.

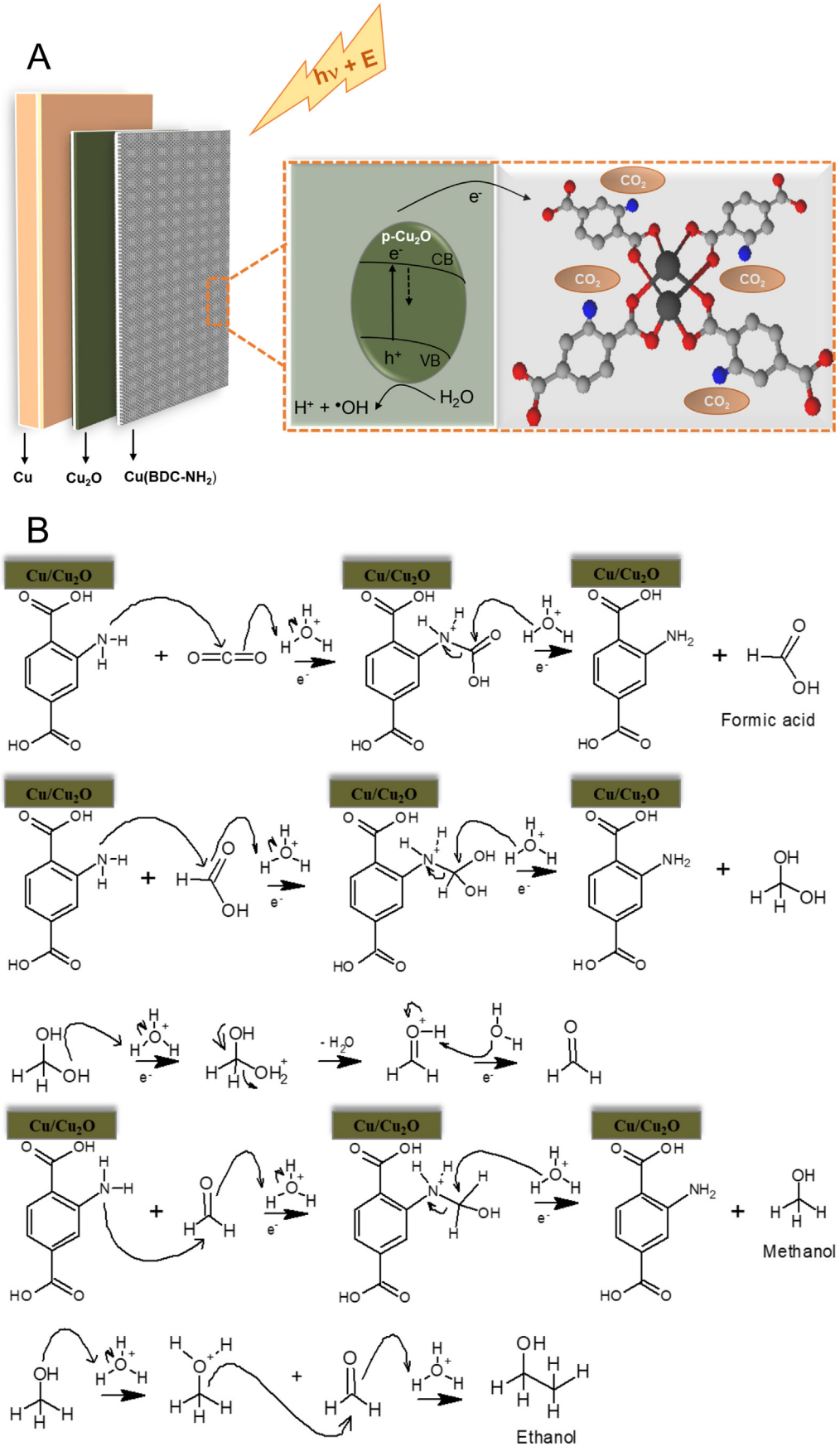

Scheme 1. (A) Representation of CO_2 capture and (B) the proposed mechanism of CO_2 photoelectroreduction with methanol and ethanol formation on Cu/Cu_2O-**Cu(BDC-NH_2)** electrodes operated under UV–Vis irradiation, with the application of an external potential.

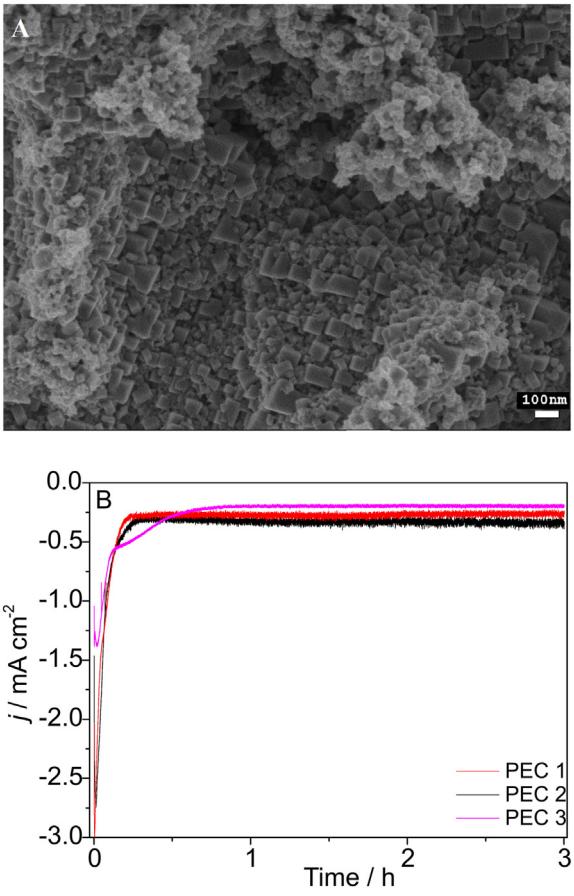

Fig. 14. A) FEG-SEM images of Cu/Cu_2O-**Cu(BDC-NH_2)** electrodes 2 after photoelectrocatalysis for 3 h under UV–Vis irradiation and in 0.1 mol L^{-1} Na_2SO_4 saturated with CO_2 at applied potential of +0.1 V. B) Amperometric behavior for reuse of Cu/Cu_2O-**Cu(BDC-NH_2)** electrode 2 after photoelectrocatalysis for 3 h under UV–Vis irradiation and in 0.1 mol L^{-1} Na_2SO_4 saturated with CO_2 at applied potentials of +0.1 V.

Declaration of Competing Interest

The authors declare that they have no known competing financial interests or personal relationships that could have appeared to influence the work reported in this paper.

Acknowledgments

The authors are grateful for the main technological support given to this work through The National Institute for Alternative Technologies of Detection, Toxicological Evaluation and Removal of Micropollutants and Radioactivies, INCT-DATREN (FAPESP #2014/50945-4; CNPq #465571/2014-0), and to Conselho Nacional de Desenvolvimento Científico e Tecnológico (CNPq) for support of this work. B.C.S received scholarships from CNPq (150223/2019-6) and K.I received scholarship from FAPESP (2017/12790-7).

References

[1] S. Neațu, J.A. Maciá-Agulló, H. Garcia, Solar light photocatalytic CO_2 reduction: general considerations and selected bench-mark photocatalysts, Int. J. Mol. Sci. 15 (2014) 5246–5262, https://doi.org/10.3390/ijms15045246.

[2] G.G. Bessegato, T.T. Guaraldo, J.F. de Brito, M.F. Brugnera, M.V.B. Zanoni, Achievements and trends in photoelectrocatalysis: from environmental to energy applications, Electrocatalysis 6 (2015) 415–441, https://doi.org/10.1007/s12678-015-0259-9.

[3] S. Xie, Q. Zhang, G. Liu, Y. Wang, Photocatalytic and photoelectrocatalytic reduction of CO_2 using heterogeneous catalysts with controlled nanostructures, Chem. Commun. 52 (2015) 35–59, https://doi.org/10.1039/C5CC07613G.

[4] S. Stülp, J.C. Cardoso, J.F. de Brito, J.B.S. Flor, R.C.G. Frem, F.A. Sayão, M.V.B. Zanoni, An artificial photosynthesis system based on Ti/TiO_2 coated with Cu(II) aspirinate complex for CO_2 reduction to methanol, Electrocatalysis 8 (2017) 279–287, https://doi.org/10.1007/s12678-017-0367-9.

[5] J.C. Cardoso, S. Stulp, M.K.R. de Souza, F.F. Hudari, J.R. Gubiani, R.C.G. Frem, M.V.B. Zanoni, The effective role of ascorbic acid in the photoelectrocatalytic reduction of CO_2 preconcentrated on TiO_2 nanotubes modified by ZIF-8, J. Electroanal. Chem. 856 (2019) 113384, https://doi.org/10.1016/j.jelechem.2019.113384.

[6] L.D.M. Torquato, F.A.C. Pastrian, J.A.L. Perini, K. Irikura, A.P.L. de Batista, A.G.S. de Oliveira-Filho, S.I. Córdoba de Torresi, M.V.B. Zanoni, Relation between the nature of the surface facets and the reactivity of Cu_2O nanostructures anchored on TiO_2NT@PDA electrodes in the photoelectrocatalytic conversion of CO_2 to methanol, Appl. Catal. B 261 (2020) 118221, https://doi.org/10.1016/j.apcatb.2019.118221.

[7] J.A.L. Perini, J.C. Cardoso, J.F. de Brito, M.V.B. Zanoni, Contribution of thin films of ZrO_2 on TiO_2 nanotubes electrodes applied in the photoelectrocatalytic CO_2 conversion, J. CO_2 Util. 25 (2018) 254–263, https://doi.org/10.1016/j.jcou.2018.04.005.

[8] J.W. Maina, C. Pozo-Gonzalo, L. Kong, J. Schütz, M. Hill, L.F. Dumée, Metal organic framework based catalysts for CO_2 conversion, Mater. Horiz. 4 (2017) 345–361, https://doi.org/10.1039/C6MH00484A.

[9] Q. Zhang, M. Chen, L. Zhong, Q. Ye, S. Jiang, Z. Huang, Highly effective removal of metal cyanide complexes and recovery of palladium using quaternary-ammonium-functionalized MOFs, Molecules 23 (2018) 2086, https://doi.org/10.3390/molecules23082086.

[10] W.-J. Li, M. Tu, R. Cao, R.A. Fischer, Metal–organic framework thin films: electrochemical fabrication techniques and corresponding applications & perspectives, J. Mater. Chem. A 4 (2016) 12356–12369, https://doi.org/10.1039/C6TA02118B.

[11] R. Ameloot, L. Stappers, J. Fransaer, L. Alaerts, B.F. Sels, D.E. De Vos, Patterned growth of metal-organic framework coatings by electrochemical synthesis, Chem. Mater. 21 (2009) 2580–2582, https://doi.org/10.1021/cm900069f.

[12] I. Buchan, M.R. Ryder, J.-C. Tan, Micromechanical behavior of polycrystalline metal–organic framework thin films synthesized by electrochemical reaction, Cryst. Growth Des. 15 (2015) 1991–1999, https://doi.org/10.1021/acs.cgd.5b00140.

[13] M. Tu, S. Wannapaiboon, R.A. Fischer, Liquid phase stepwise growth of surface mounted metal–organic frameworks for exploratory research and development of applications, Inorg. Chem. Front. 1 (2014) 442–463, https://doi.org/10.1039/C4QI00037D.

[14] Y. Wang, T. Chu, M. Yu, H. Liu, Y. Yang, One step cathodically electrodeposited [Tb2(BDC)3(H2O)4]n thin film as a luminescent probe for Cu2+ detection, RSC Adv. 4 (2014) 58178–58183, https://doi.org/10.1039/C4RA09387A.

[15] L. Fotouhi, M. Naseri, Recent electroanalytical studies of metal-organic frameworks: a mini-review, Crit. Rev. Anal. Chem. 46 (2016) 323–331, https://doi.org/10.1080/10408347.2015.1063978.

[16] M. Li, M. Dincă, Selective formation of biphasic thin films of metal–organic frameworks by potential-controlled cathodic electrodeposition, Chem. Sci. 5 (2013) 107–111, https://doi.org/10.1039/C3SC51815A.

[17] Y. Dou, J. Zhou, A. Zhou, J.-R. Li, Z. Nie, Visible-light responsive MOF encapsulation of noble-metal-sensitized semiconductors for high-performance photoelectrochemical water splitting, J. Mater. Chem. A 5 (2017) 19491–19498, https://doi.org/10.1039/C7TA06443H.

[18] X. Zhang, T. Lei, Y. Liu, J. Qiao, Enhancing CO_2 electrolysis to formate on facilely synthesized Bi catalysts at low overpotential, Appl. Catal. B Environ. 218 (2017) 46–50, https://doi.org/10.1016/j.apcatb.2017.06.032.

[19] J. Zhou, A. Zhou, L. Shu, M.-C. Liu, Y. Dou, J.-R. Li, Cellular heterojunctions fabricated through the sulfurization of MOFs onto ZnO for high-efficient photoelectrochemical water oxidation, Appl. Catal. B Environ. 226 (2018) 421–428, https://doi.org/10.1016/j.apcatb.2017.12.065.

[20] S. Zhou, P. Yue, J. Huang, L. Wang, H. She, Q. Wang, High-performance photoelectrochemical water splitting of $BiVO_4$@Co-MIm prepared by a facile in-situ deposition method, Chem. Eng. J. 371 (2019) 885–892, https://doi.org/10.1016/j.cej.2019.04.124.

[21] D. Cardenas-Morcoso, R. Ifraemov, M. García-Tecedor, I. Liberman, S. Gimenez, I. Hod, A metal–organic framework converted catalyst that boosts photo-electrochemical water splitting, J. Mater. Chem. A 7 (2019) 11143–11149, https://doi.org/10.1039/C9TA01559K.

[22] R. Tang, S. Zhou, H. Li, R. Chen, L. Zhang, L. Yin, Halogen bonding induced aqueously stable $CsPbBr_3$@MOFs-derived Co_3O_4/N-doped-C heterostructure for high-performance photoelectrochemical water oxidation, Appl. Catal. B Environ. 265 (2020) 118583, https://doi.org/10.1016/j.apcatb.2019.118583.

[23] J. Cheng, X. Xuan, X. Yang, J. Zhou, K. Cen, Preparation of a Cu(BTC)-rGO catalyst loaded on a Pt deposited Cu foam cathode to reduce CO_2 in a photoelectrochemical cell, RSC Adv. 8 (2018) 32296–32303, https://doi.org/10.1039/C8RA05964K.

[24] J.C. Cardoso, S. Stulp, J.F. de Brito, J.B.S. Flor, R.C.G. Frem, M.V.B. Zanoni, MOFs based on ZIF-8 deposited on TiO_2 nanotubes increase the surface adsorption of CO_2 and its photoelectrocatalytic reduction to alcohols in aqueous media, Appl. Catal. B Environ. 225 (2018) 563–573, https://doi.org/10.1016/j.apcatb.2017.12.013.

[25] X. Deng, R. Li, S. Wu, L. Wang, J. Hu, J. Ma, W. Jiang, N. Zhang, X. Zheng, C. Gao, L. Wang, Q. Zhang, J. Zhu, Y. Xiong, Metal–organic framework coating enhances the performance of Cu_2O in photoelectrochemical CO_2 reduction, J. Am. Chem. Soc. 141 (2019) 10924–10929, https://doi.org/10.1021/jacs.9b06239.

[26] J. Wang, C. Xue, W. Yao, J. Liu, X. Gao, R. Zong, Z. Yang, W. Jin, D. Tao, MOF-derived hollow TiO_2@C/$FeTiO_3$ nanoparticles as photoanodes with enhanced full spectrum light PEC activities, Appl. Catal. B Environ. 250 (2019) 369–381, https://doi.org/10.1016/j.apcatb.2019.03.002.

[27] I. Stassen, M. Styles, T. Van Assche, N. Campagnol, J. Fransaer, J. Denayer, J.-C. Tan, P. Falcaro, D. De Vos, R. Ameloot, Electrochemical film deposition of the zirconium metal–organic framework UiO-66 and application in a miniaturized sorbent trap, Chem. Mater. 27 (2015) 1801–1807, https://doi.org/10.1021/cm504806p.

[28] P. Mosae Selvakumar, S. Nadella, J. Sahoo, E. Suresh, P.S. Subramanian, Copper(II) bischelate paddle wheel complex and its bipyridine/phenanthroline adducts, J. Coord. Chem. 66 (2013) 287–299, https://doi.org/10.1080/00958972.2012.755521.

[29] B.C. Silva, K. Irikura, J.B.S. Flor, R.M.M. dos Santos, A. Lachgar, R.C.G. Frem, M.V.B. Zanoni, Electrochemical preparation of Cu/Cu_2O-Cu(BDC) metal-organic framework electrodes for photoelectrocatalytic reduction of CO_2, J. CO_2 Util. 42 (2020) 101299, https://doi.org/10.1016/j.jcou.2020.101299.

[30] A. Dhakshinamoorthy, Z. Li, H. Garcia, Catalysis and photocatalysis by metal organic frameworks, Chem. Soc. Rev. 47 (2018) 8134–8172, https://doi.org/10.1039/C8CS00256H.

[31] Z. Xiang, S. Leng, D. Cao, Functional group modification of metal–organic frameworks for CO_2 capture, J. Phys. Chem. C 116 (2012) 10573–10579, https://doi.org/10.1021/jp3018875.

[32] H.M. Lee, I.S. Youn, M. Saleh, J.W. Lee, K.S. Kim, Interactions of CO_2 with various functional molecules, Phys. Chem. Chem. Phys. 17 (2015) 10925–10933, https://doi.org/10.1039/C5CP00673B.

[33] R. Vaidhyanathan, S.S. Iremonger, G.K.H. Shimizu, P.G. Boyd, S. Alavi, T.K. Woo, Direct observation and quantification of CO_2 binding within an amine-functionalized nanoporous solid, Science 330 (2010) 650–653, https://doi.org/10.1126/science.1194237.

[34] M.V.B. Zanoni, J.J. Sene, M.A. Anderson, Photoelectrocatalytic degradation of Remazol Brilliant Orange 3R on titanium dioxide thin-film electrodes, J. Photochem. Photobiol. A Chem. 157 (2003) 55–63, https://doi.org/10.1016/S1010-6030(02)00320-9.

[35] D. Sun, Y. Fu, W. Liu, L. Ye, D. Wang, L. Yang, X. Fu, Z. Li, Studies on photocatalytic CO_2 reduction over NH_2-UiO-66(Zr) and its derivatives: towards a better understanding of photocatalysis on metal–organic frameworks, Chem. Eur. J. 19 (2013) 14279–14285, https://doi.org/10.1002/chem.201301728.

[36] J. Lu, M. Liu, S. Zhou, X. Zhou, Y. Yang, Electrospinning fabrication of $ZnWO_4$ nanofibers and photocatalytic performance for organic dyes, Dyes Pigments 136 (2017) 1–7, https://doi.org/10.1016/j.dyepig.2016.08.008.